ACS SENSORS

pubs.acs.org/acssensors Article

Implantable Self-Reporting Stents for Detecting In-Stent Restenosis and Cardiac Functional Dynamics

Nomin-Erdene Oyunbaatar, Dong-Su Kim, Arunkumar Shanmugasundaram, Su-Hwan Kim, Yun-Jin Jeong, Juyeong Jo, Kyeongha Kwon, Eunpyo Choi, and Dong-Weon Lee*

Cite This: *ACS Sens.* 2023, 8, 4542−4553 Read Online

ACCESS | Metrics & More | Article Recommendations | Supporting Information

ABSTRACT: Despite the increasing number of stents implanted each year worldwide, patients remain at high risk for developing in-stent restenosis. Various self-reporting stents have been developed to address this challenge, but their practical utility has been limited by low sensitivity and limited data collection. Herein, we propose a next-generation self-reporting stent that can monitor blood pressure and blood flow inside the blood arteries. This proposed self-reporting stent utilizes a larger inductor coil encapsulated on the entire surface of the stent strut, resulting in a 2-fold increase in the sensing resolution and coupling distance between the sensor and external antenna. The dual-pressure sensors enable the detection of blood flow in situ. The feasibility of the proposed self-reporting stent is successfully demonstrated through in vivo analysis in rats, verifying its biocompatibility and multifunctional utilities. This multifunctional self-reporting stent has the potential to greatly improve cardiovascular care by providing real-time monitoring and unprecedented insight into the functional dynamics of the heart.

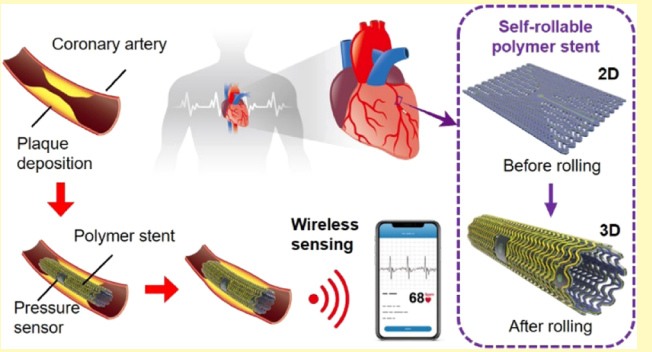

KEYWORDS: *smart stent, restenosis, pressure sensor, wireless resonance, blood flow sensor*

Cardiovascular diseases (CVDs) are among the leading causes of mortality, accounting for 30% of the total deaths globally.[1,2] The main cause of CVD is atherosclerosis, which is usually associated with plaque formation inside the arteries. Arterial plaques can lead to thrombosis and major heart damage.[3,4] Implanting a vascular stent at the lesion site is currently the most effective method for reopening obstructed arteries in advanced atherosclerosis. Several generations of cardiovascular stents have been developed throughout the years to improve patient outcomes and reduce postimplantation complications, such as restenosis. Stent technology has been constantly evolving from bare-metal stents to drug-eluting stents and to bioresorbable stents.[5−11] However, currently available stents fall short of providing permanent protection against restenosis. Studies report an increase in late-stage thrombosis after depletion of the drug reservoir. The procedures required for the detection of restenosis, such as angiography and duplex ultrasonography, are not employed until particular symptoms such as chest discomfort are observed, at which point the blockage of the arteries may have already advanced.[12−14] Besides, these techniques are not readily implemented, as they require hospitalization and have high costs. Therefore, the development of stents that can continually monitor blood pressure and other functional dynamics of the heart is highly desirable for the early detection of restenosis and to minimize the risk of CVD.

Recently, the use of self-reporting stents for the early detection of restenosis has received considerable attention. Such devices are capable of collecting cardiovascular health-associated data autonomously and reporting the information to healthcare providers, thereby improving patient outcomes and facilitating personalized treatment.[15−18] These developments are particularly beneficial, as they allow the early detection of restenotic lesions, enabling timely interventions to prevent blood clots and other complications. The proposed self-reporting stents utilize various technologies including piezo-resistive sensors, magnetoelastic resonators, and microelectromechanical system (MEMS)-based LC-capacitive pressure sensors for continuous monitoring of arterial blood pressure.[19−21] Capacitive pressure sensors have gained more attention over the piezo-resistive and magnetoelastic resonators owing to their high sensitivity and low-power

Received: June 29, 2023
Revised: October 6, 2023
Accepted: November 9, 2023
Published: December 5, 2023

consumption. Besides, self-reporting stents with integrated capacitive pressure sensors can detect biological signals without requiring an additional power source and communicate with an external device through an embedded MEMS-based pressure sensor.[22,23] For instance, Takahata et al. generated a self-reporting stent with an integrated silicon-based MEMS capacitive pressure sensor for real-time pressure monitoring in the arteries.[24] Park et al. developed a biocompatible, polycaprolactone-based, three-dimensional (3D)-printed polymer stent with an integrated capacitive pressure sensor;[25] the self-reporting stent was generated by manually attaching a capacitive pressure sensor to the stent using an adhesive. The integration of a sensor using an adhesive increases the layer thickness in the bonded region, which may impede blood flow, and the sensor may be destroyed during crimping.[26] Herbert et al. demonstrated a fully implantable soft electronic system that lacks batteries and circuits. Yet, the smart stent can continuously monitor restenosis wirelessly in real time using nanomembrane strain sensors within an electronic stent.[27] Chen et al. developed a self-reporting stent for wireless monitoring of intravascular pressure.[28] However, the proposed self-reporting stent did not perform well in vivo as the sensor was distorted from the epoxy joint during the crimping and balloon expansion process. This problem was addressed by the same group in a later study by integrating the capacitive sensor into the stent using a microlaser welding technique.[29] Nevertheless, the captive pressure sensor was produced by connecting the inductor coil and capacitor plate by using a tiny gold wire, limiting its real-time applicability. In our prior research endeavor, we successfully engineered an innovative self-rolling, self-reporting intelligent stent designed specifically for monitoring in-stent restenosis.[20,30] While conducting in vitro experiments, we observed that the aforementioned self-reporting stent exhibited promising responsiveness to biosignals. However, its practical utility was limited due to the restricted transmission range of the signals caused by the utilization of smaller inductor coils.[31−33] Consequently, there exists a pressing need to devise a swift and conveniently accessible self-reporting stent possessing superior wireless sensing capabilities to facilitate enhanced surveillance of cardiovascular well-being.

The feasibility of a self-reporting stent largely depends on the external antenna reading distance, which is a crucial parameter for its application to the cardiovascular system. In prior self-reporting stent designs, a small inductor area was used, resulting in limited sensing resolution due to the low number of inductor coils. In addition, currently available self-reporting stents can continuously monitor blood pressure but not blood flow. To overcome this limitation, herein, we propose a new strategy to develop a self-reporting stent for detecting in-stent restenosis by monitoring blood pressure and blood flow inside the arteries. The shortcoming of low sensing resolution was overcome by incorporating the inductor structure into the entire area of the stent struts. This design enabled the integration of a large number of inductor coils, which improved the sensing resolution. The continuous monitoring of blood flow provides real-time data on blood pressure, allowing the early detection of changes potentially indicative of underlying health issues. The use of stents to monitor blood pressure has several advantages over traditional monitoring methods, including reduced invasiveness, continuous monitoring, and improved accuracy. To continuously measure blood flow, we proposed a dual-pressure-sensor-infused self-reporting stent design. This design was successfully realized through the implementation of a larger inductor coil, enabling the integration of two pressure sensors into a single self-reporting stent. The dual-sensor-infused self-reporting stent enhanced the precision and reliability of the obtained data. The feasibility of the proposed self-reporting stent was evaluated by measuring the blood pressure and heart rate by implanting the self-reporting stent into the blood arteries of a 3D-printed phantom mimicking the human heart. Finally, the in vivo analysis in rats demonstrated the biocompatibility and multifunctional utilities of the proposed implantable self-reporting stent.

MATERIALS AND METHODS

Fabrication of the Self-Reporting Stent. The detailed fabrication process of the self-reported stent is illustrated in Figure S1. The self-reporting stent was generated through a process involving a top capacitor plate, a bottom capacitor plate with an inductor coil, and the steps of thermal bonding and releasing. First, a 300 nm silicon dioxide (SiO_2) sacrificial layer was formed on a 4 in. silicon wafer through a wet oxidation process at 1000 °C for 40 min. A 10 μm thick SU-8 3010 was spin-coated on the SiO_2 sacrificial layer at 2400 rpm for 40 s. The SU-8 layer was then patterned with 10 nm thick and 100 nm thick titanium and chromium layers using DC sputtering at 50 W for 1 h. The 2 μm thick SU-8 3010 was coated on the titanium and chromium layers to encapsulate the electrode materials. The top side of the SU-8 encapsulation layer contained a tiny open area for the electrical connection. Subsequently, a 10 μm thick PermiNex was coated on top of the SU-8 encapsulation layer, providing an air cavity and electrical connection points. Finally, the top capacitor plate layer was released from the silicon wafer by dissolving the SiO_2 sacrificial layer using a buffered hydrofluoric acid (BHF) solution, as shown in Figure S1a.

The bottom capacitor plate with an inductor coil was fabricated on a 4 in. silicon wafer. First, a 300 nm thick SiO_2 sacrificial layer was formed on a silicon wafer as described above. Then, using a modified photolithographic technique, a 2 μm thick SU-8 pattern (breadth, 13 mm; length, 18 mm) was created on a SiO_2 sacrificial layer. Subsequently, 10 nm thick and 200 nm thick Ti and Cu layers were deposited on the SU-8 pattern by DC sputtering. Then, the AZ P4620 photoresist was spin-coated on the Ti/Cu layers at 1500 rpm for 30 s. The photoresist was soft-backed at 110 °C for 80 s followed by ultraviolet (UV) curing (9.5 mJ/cm^2) for 90 s. Then, the photoresist was developed for 2 min using an AZ 340 developer. Next, a 10 μm thick Cu layer was electroplated on the SU-8 stent mesh structure with the same pattern using thick AZ4620, which acts as an inductive layer. Finally, the SU-8 negative photoresist with a thickness of 10 μm was removed from the silicon wafer by dissolving the SiO_2 sacrificial layer using a BHF solution, as shown in Figure S1b. The top and bottom capacitor plates with inductor coils were precisely aligned using a modified mask aligner and bonded together to obtain the LC-pressure sensor-integrated two-dimensional (2D) self-reporting stent mesh structure through a hot-pressing technique with an applied force of 10 kN at 150 °C for 30 s, as shown in Figure S1c. The self-assembled self-reporting stent with an integrated LC-pressure sensor was produced from the 2D self-reporting stent mesh structure through thermally induced surface stress at 250 °C for 3 min (Figure S1d). We utilized temperature-induced surface stress to fabricate a self-rolling structure. Therefore, the effect of the temperature on the stent diameter was investigated as shown in Figure S2.

Experimental Procedures and Measurements. The fidelity of the fabricated self-assembled self-reporting stent was investigated by field emission scanning electron microscopy (FE-SEM; JEOl, JSM-7900F). The radial force of the self-reporting stent was determined by using a universal tensile machine (Shimadzu, EZ-L). The changes in the capacitance of the self-reporting stent under the indicated levels of applied pressure were measured using an LCR meter (KeySight, E4980AL). The corresponding displacement of the capacitor plates

https://doi.org/10.1021/acssensors.3c01313
ACS Sens. 2023, 8, 4542−4553

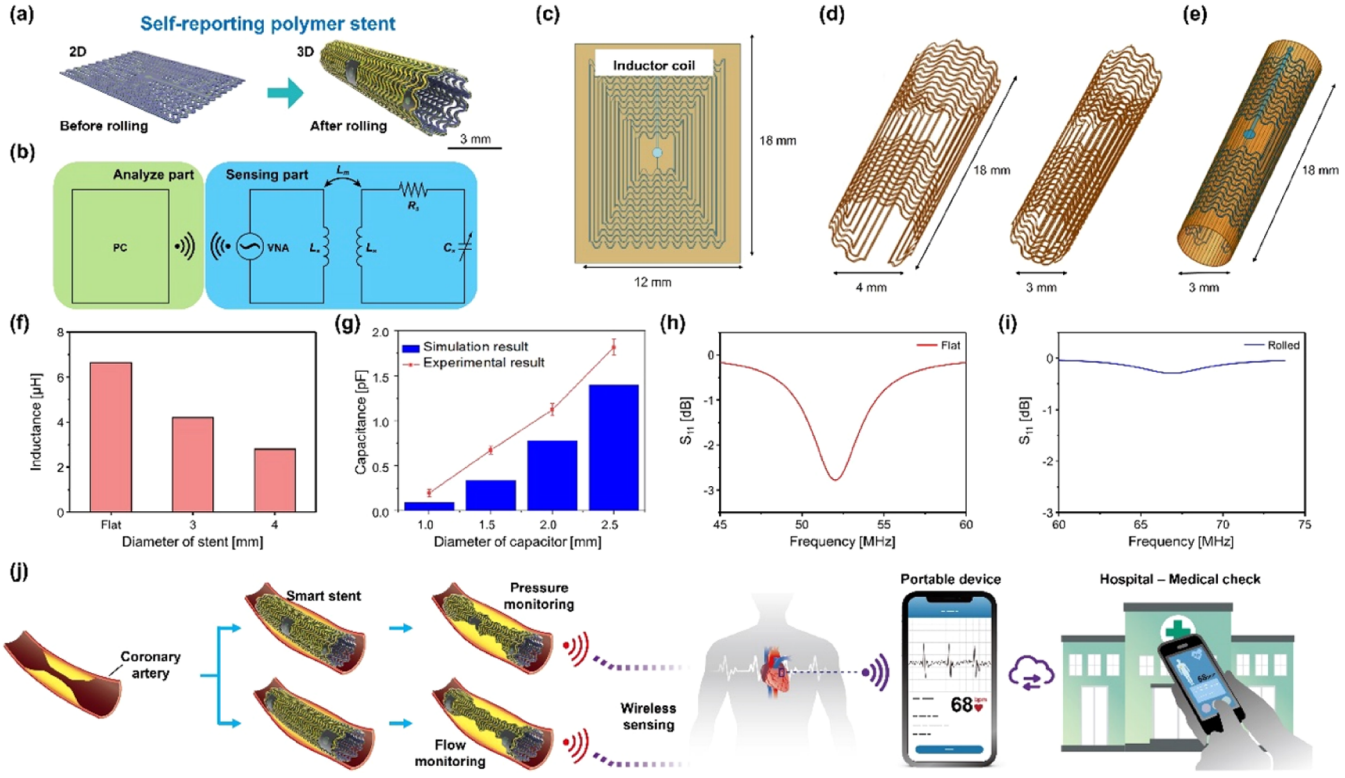

Figure 1. Conceptual schematic illustrating the design and function of the self-reporting stent. (a, b) Device concept and working mechanism of the proposed self-reporting stent. Finite element method (FEM) simulation analysis of a planar inductor coil with a two-dimensional design and its self-assembled 3D structure with a 3 mm radius was used to determine the electrical parameters of the proposed device. (c) The 2D planar structure of the LC-pressure sensor-integrated self-reporting stent mesh with a breadth of 18 mm and a length of 12 mm. (d) The rolled state of the inductor coil, with a diameter of 4 or 3 mm. (e) The 3D structure of the LC-pressure sensor-integrated self-reporting stent mesh with a length of 12 mm and a diameter of 3 mm. (f) The FEM simulation of the resonance frequency of the LC-pressure sensor-integrated self-reporting stent with a diameter of 3 and 4 mm before and after the self-assembly process. (g) The FEM simulation and experimental data of the capacitance of the LC-pressure sensor-integrated self-reporting stent at different applied capacitor diameters. (h, i) The resonance frequency of the self-reporting stent before and after the self-assembly process. (j) The schematic shows the self-reporting stent before and after the self-assembly process. The proposed self-reporting stent is designed to be implanted within a blood artery at a specified stenosis site to detect and report through wireless signaling the occurrence of in-stent restenosis. Stent restenosis is caused by the formation of scar tissue or the proliferation of smooth muscle cells within the stent. The narrowing of the blood vessel leads to an increase in local blood pressure, a reduction in blood flow, and a shift in the resonance frequency. The resonant frequency of the self-reporting stent is continuously monitored by a wireless reader, which can detect any deviation from the expected frequency and send an alert to the patient or healthcare provider, indicating potential restenosis. This allows for early detection and prompt treatment to prevent further deterioration of the blood flow through the affected vessel.

was measured using a laser vibrometer (OFV-5000, OFV-534, OFV-505, Polytec, South Korea). The resonance frequency of the LC-pressure sensor-integrated self-reporting stent under pressure and in the indicated environmental settings was investigated using a vector network analyzer (N9913B, KeySight).

In Vivo Demonstration. The experiment was conducted in accordance with the ethical guidelines #CNU IACUC-YB-2022−77 approved by the Animal Ethics Committee at Chonnam National University and relevant national laws. The self-reporting stent was implanted into the femoral artery of the SD rat using tissue adhesive biological glue (Histoacryl, B. Braun, Germany). For detecting the highly sensitive CRP, the serum samples were separated from the blood, and the CRP levels were quantified and analyzed at the Seegene Medical Foundation (South Korea).

RESULTS AND DISCUSSION

The device concept and working mechanism of the proposed self-reporting stent are schematically illustrated in Figure 1a. The detailed fabrication process of the self-reporting stent is described in the Materials and Methods Section. A dual wireless pressure sensor was integrated into a stent using advanced modified photolithography and thermocompression bonding techniques. These techniques allowed for the precise and controlled placement of the wireless pressure sensors, ensuring their optimal performance. The self-assembly process involves the use of thermal treatment and residual stress to transform a two-dimensional (2D) planar structure into a complex 3D stent structure. The self-reporting stent comprises a stent and a dual wireless pressure sensor that is inductively coupled with an external vector network analyzer (VNA).

The pressure sensor enables the device to measure and report any changes in the functional dynamics of the heart. This information can be transmitted wirelessly to the VNA, providing healthcare professionals with real-time data on the performance of the stent and the patient's condition (Figure 1b). The parameters of inductance and resonance frequency of a self-reporting stent with an integrated LC-pressure sensor were simulated to better understand the effect of the self-rolling process on the inductance of the self-reporting stent. The finite element method (FEM) simulation was carried out using the software Ansys HFSS 2021 version R1. The geometry of the stent was determined through an automatic meshing procedure on HFSS, while the mesh distribution was

https://doi.org/10.1021/acssensors.3c01313
ACS Sens. 2023, 8, 4542−4553

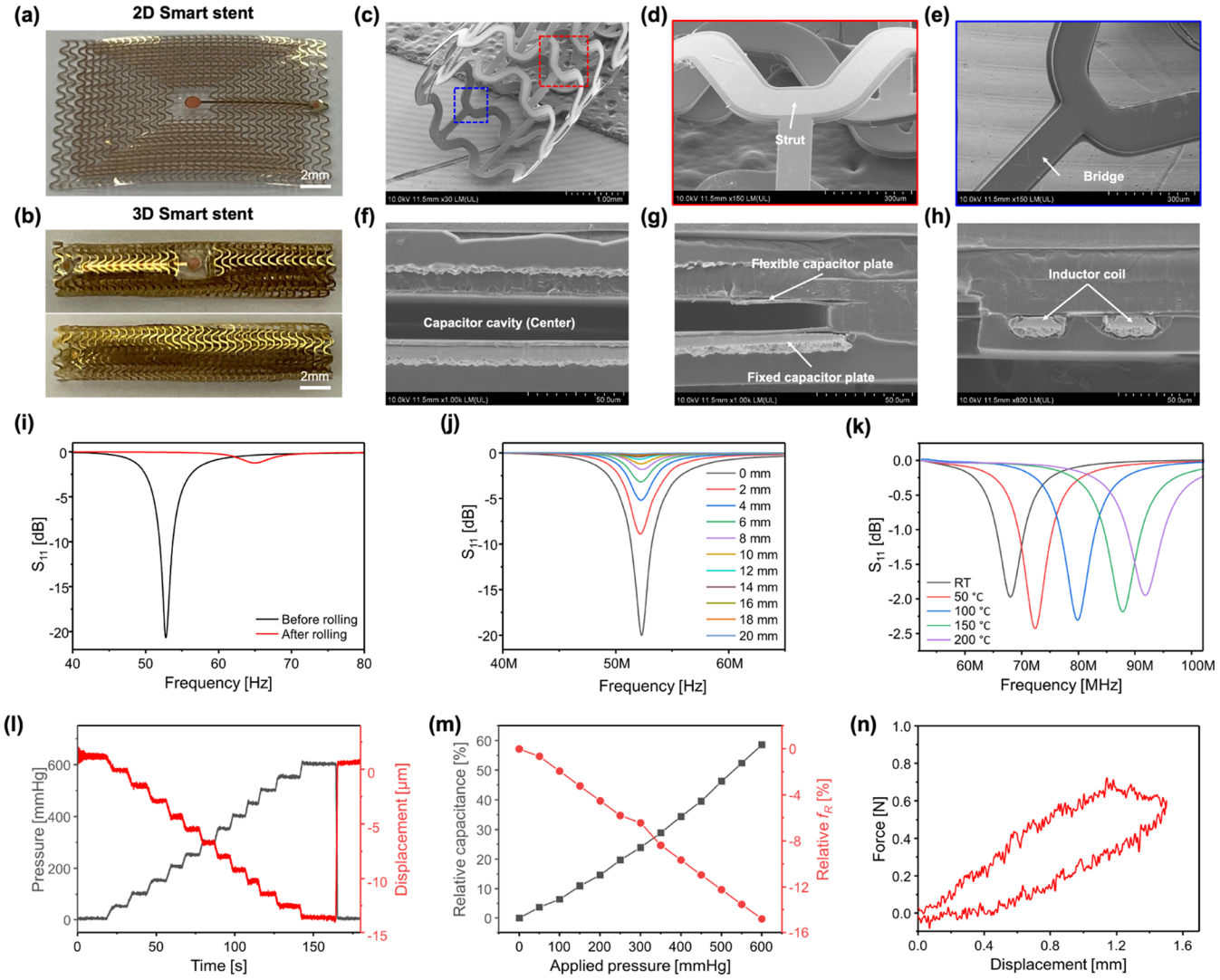

Figure 2. Morphological fidelity and preliminary characteristics of the self-reporting stent. (a, b) Optical images of the fabricated self-reporting stent before and after self-assembly. (c–h) Field emission scanning electron micrographs and cross-sectional view of the fabricated self-reporting stent, showing the stent strut, bridge, and encapsulated inductor coil and capacitor cavity of the self-reporting stent. (i) Resonance frequency of the self-reporting stent before and after self-assembly. (j, k) Resonance frequency of the stent as a function of the external antenna working distance and temperature. (l) Relationship between the applied pressure and the capacitor plate displacement. (m) Effect of applied pressure on the relative capacitance and resonance frequency of the self-reporting stent. (n) Radial force of the LC-pressure sensor-integrated self-reporting stent.

adjusted manually to ensure accuracy. The simulation process involved the iterative steps of meshing, solving, increasing meshing, solving, checking converge, increasing mesh density, solving, checking convergence, and repeating until a desired accuracy was reached. To check the convergence, delta S was set at 0.01 or 0.02. The mesh distribution was performed manually to obtain the stent mesh design precisely. Reliability of the simulation data depends on the accuracy of electrical parameters such as conductivity, permittivity, loss tangent, and capacitance of the design material. As these properties exhibit frequency dependence, the simulation results can be highly accurate if the electrical parameters are defined at the frequency of solution, highlighting the importance of considering the frequency-dependent electrical properties of the design material in obtaining reliable simulation data. To effectively investigate the impact of misalignment between the self-reporting stent and the external pick-up coil on the resonance frequency, we conducted a FEM analysis. The FEM simulation data, presented in Figure S3, demonstrate that the S_{11} dip weakens as the misalignment distance increases. Thus, it is imperative to ensure precise alignment of the coil-sensor to maximize sensing performance.

A planar inductor coil with a two-dimensional geometry, featuring dimensions of 12 mm in breadth and 18 mm in length, was employed in the simulation of electrical properties, as shown in Figure 1c. Both the planar 2D configuration and the self-assembled 3D structure (with diameters of 3 and 4 mm) of the self-reporting stent's inductor coil were simulated (Figure 1d,e). The change in inductance due to self-assembly within the mesh structure was examined, as demonstrated in Figure 1f. A negative correlation was observed between the stent mesh inductance and the bending angle. The planar 2D mesh structure exhibited a simulated inductance of 6.65 μH, while the 3D stent structures with diameters of 4 and 3 mm showed inductances of 4.2 and 2.8 μH, respectively. The inductance of the 2D mesh structure was measured by using an LCR meter, and the experimentally obtained result was 6.53 μH, which represents an ~2% error between the simulation

https://doi.org/10.1021/acssensors.3c01313
ACS Sens. 2023, 8, 4542−4553

and experimental results. The capacitance of the capacitor was simulated and experimentally measured as a function of its diameter, revealing an increase in capacitance with an expanding diameter (Figure 1g). The experimental result is slightly higher than the simulated data, which is the influence of the flexible membrane deflection during thermal bonding. The simulated resonant frequencies of the LC-pressure sensor-integrated self-reporting stent, both pre- and post-self-assemblies (with a diameter of 4 mm), were determined to be 52 and 67 MHz, respectively (Figure 1h,i). The self-reported stent was fabricated with the desired dimensions and electrical parameters in accordance with the simulation parameters that were used as the basis for its design. The proposed self-reporting stent with the dual wireless pressure sensor can be positioned at the site of stenosis in the blood artery. Local blood pressure varies because of restenosis within the stent, and as a result, the resonance frequency of the self-reporting stent shifts. The change in resonance frequency of the self-reporting stent can be continuously monitored in real time using a wireless reader, which alerts the patient and sends information to the physician whenever restenosis occurs, as shown in Figure 1j.

The top and bottom capacitor plates along with the inductor coil were bonded together using a thermal hot-pressing technique, applying a force of 10 kN at 150 °C for 30 s. The bonding process, which entails an exposure to high temperature and pressure, resulted in an unintended deformation of the capacitor plates, as depicted in Figure S4. This deformation can potentially cause substantial errors in the real-time measurement of biosignals. The introduction of such errors would negatively impact the accuracy of the readings, compromising the validity of the reported data. Therefore, we first evaluated the effect of applied pressure on the capacitance of the capacitor (Figure S5). Optical and surface profile images of the fabricated capacitor plates before and after the thermal press bonding are shown in Figure S5a. A surface profiler was utilized for examining the topography of flexible capacitor surfaces. No noticeable variations in the surface profile images before and after the thermal pressing process were detected, suggesting that the application of high temperature and pressure did not alter the internal geometry of the capacitor plates, which demonstrates the robustness and reliability of the fabrication process. The displacement of the flexible capacitor and the corresponding changes in capacitance were measured using an LAB-view-assisted laser vibrometer and an LCR meter with a two-point probe, as shown in Figure S5b. The displacement of the flexible capacitor plate was measured under various pressures (range of 0−300 mmHg; Figure S5c). External pressure was applied to the center of the capacitor diaphragm, and the resulting change in capacitance was measured. The distance between the capacitor plates decreased with an increase in pressure and returned to its initial level when the pressure was removed (Figure S5d). The maximum capacitor plate displacement was about 6.2 μm when the applied pressure reached 300 mmHg. We also investigated in detail the capacitor plate displacement and the corresponding changes in capacitance at applied pressures of 0−300 mmHg. The measured base capacitance of the capacitor was 0.6 pF, which matches exactly with its theoretical value. When the displacement increased by 38%, the capacitance increased by about 30%, reflecting the reliability of the proposed sensor.

The microstructure and fidelity of the fabricated self-reporting stent were assessed by using optical analysis and field emission scanning electron microscopy (FE-SEM). Optical micrographs of the stent before and after the self-assembly process exhibited no evidence of physical damage (Figure 2a,b). The heat-induced self-assembly did not affect the structural integrity of the stent strut, and the LC-pressure sensor maintained its uniform geometry throughout the process. FE-SEM analysis verified the formation of a strut with a consistent width and thickness (Figure 2c). Higher-magnification images further substantiated the high fidelity of the strut and bridge within the self-reported stent (Figure 2d,e). Cross-sectional microstructural views of the fabricated stent were also examined using FE-SEM, revealing encapsulated copper inductor coils, capacitor plates, and a cavity within the self-reporting stent. The air cavity of the capacitor exhibited a diameter of 10 μm (Figure 2f). The thermal pressing and heating procedures employed to convert the 2D flat mesh into the 3D self-assembled stent structure did not produce any discernible physical damage to the inductor coils or capacitor plates (Figure 2g). Magnified FE-SEM images further corroborated the uniform shape and size of the encapsulated inductor coils and capacitor plates (Figure 2h). The resonance frequency of the stent was measured before and after self-assembly using an external antenna connected to a vector network analyzer and was found to increase from 52 to 67 MHz after self-assembly (Figure 2i). The self-assembly process not only increased the resonance frequency of the self-reporting stent but also decreased the intensity of the resonance frequency due to the electrical characteristics of bent inductor coils, which also affect the shift of the resonance frequency. The increase in the resonance frequency of the self-reporting stent can also be attributed to the decreased distance between the capacitor plates during the transformation of a 2D planar mesh to a 3D stent structure, thereby increasing the capacitance and resonance frequency of the self-reporting stent.

The resonance frequency of a self-reporting stent with varying numbers of turns in its inductor coil (10, 15, 20, and 25 turns) and the effect of the external antenna reading distance on the resonance frequency of the self-reporting stent were investigated, as shown in Figure S6. To assess this, the external antenna working distance was systematically increased from 2 to 20 mm (2 mm increments) in the radial direction of the self-reporting stent. Increasing the number of inductor coil turns resulted in corresponding increases in the intensity of resonance frequency. The self-reporting stent with 25 turns induced a nearly 20-fold increase in intensity compared to the 10-turn inductor coil variant. Despite the decrease in the resonance frequency with an increasing working antenna distance, the self-reporting stent still exhibited remarkable sensitivity, as the reader was able to detect the resonance frequency even at a distance of 20 mm, likely due to the larger inductor coil encased within the self-reporting stent (Figure 2j).

Evaluating the impact of the temperature on the resonance frequency of the self-reporting stent is essential for comprehending its functionality and refining its design (Figure 2k). Therefore, we evaluated the resonance frequency of the self-reporting stent at different temperatures. The resonance frequency of the self-reporting stent increases with external temperature due to the temperature-dependent properties of the materials constituting the stent and its embedded components, such as the inductor coil and capacitor. For instance, the copper inductor coil exhibits an increase in

https://doi.org/10.1021/acssensors.3c01313
ACS Sens. 2023, 8, 4542−4553

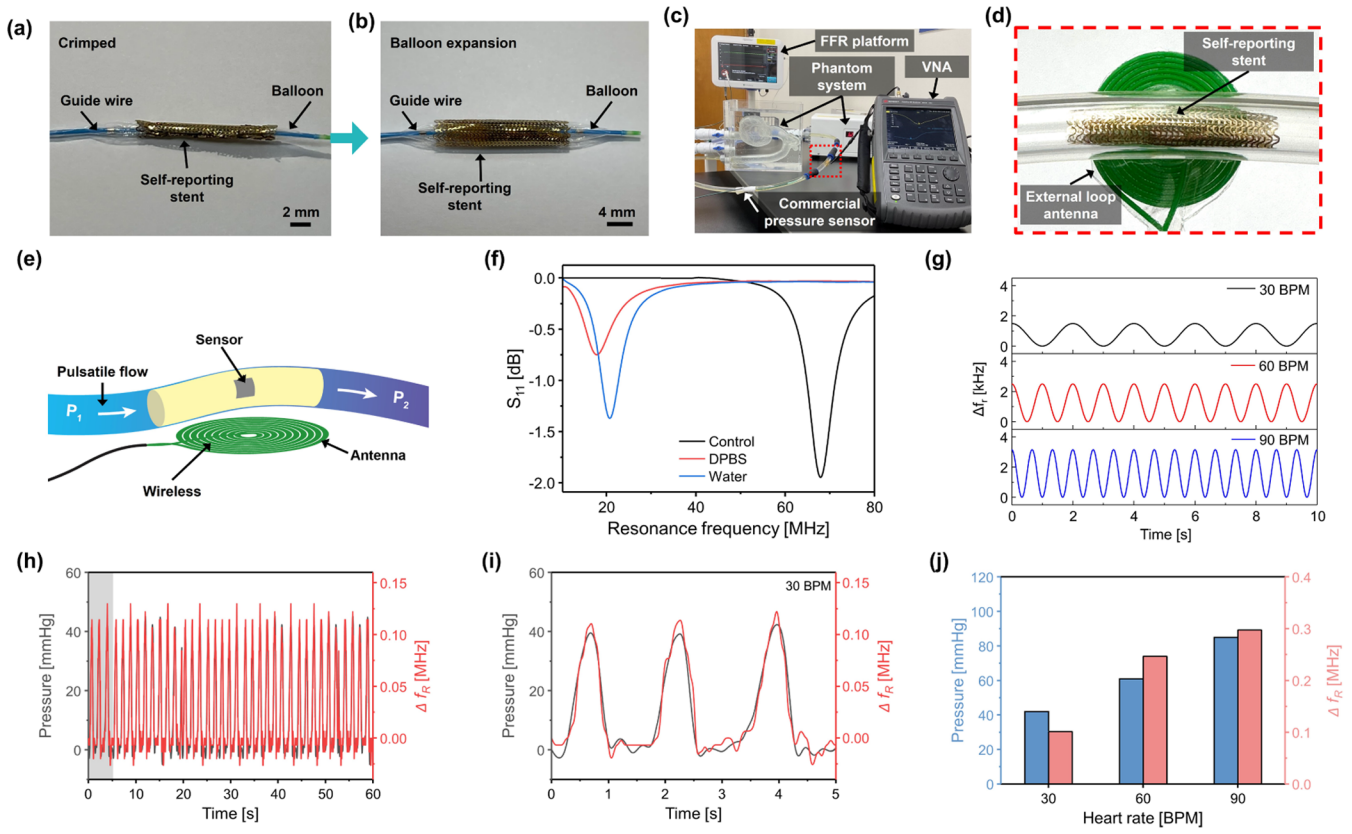

Figure 3. In vitro phantom experiment demonstrated the practical feasibility of the proposed self-reporting stent. (a, b) Photograph shows the self-reporting stent in crimping and balloon expansion states. (c) The fractional flow reserve-controlled customized phantom system was utilized to measure biological cues such as blood pressure using the fabricated self-reporting stent. (d) A closer view of the artificial blood arteries implanted with a self-reporting stent connected to an external wireless reader. (e) Schematic shows the experimental procedure used for the measurement of biological cues. (f) Resonance frequency of the self-reporting stent in deionized water and Dulbecco's phosphate-buffered saline solution. (g) Resonance frequency of the self-reporting stent at different beat rates. (h) Relationship between the applied pressure and the change in resonance frequency of the self-reporting stent at 30 bpm. (i) Enlarged region shows the change in the resonance frequency of the self-reporting stent at 30 bpm. (j) The bar plot shows the pressure and change in resonance frequency of the self-reporting stent at 30, 60, and 90 bpm.

electrical resistivity with increasing temperature. This increase in resistivity can lead to a higher series resistance in the coil, which in turn affects the inductance and the overall resonant frequency. Additionally, the air cavity distance between the capacitor plate decreases with increasing external temperature, leading to a decrease in the capacitor and an increase in the resonance frequency. The effect of externally applied pressure on the capacitor plate displacement, and its subsequent effects on the relative capacitance and resonance frequency, was examined at varying pressure levels. The self-reporting stent was positioned within a tube, with one end connected to a plastic syringe to apply external pressure and the opposite end connected to an external pressure gauge (MS-TECH, South Korea) for monitoring the internal pressure within the chamber. A schematic representation of the experimental setup employed to investigate the impact of the externally applied pressure on the self-reporting stent's resonance frequency is depicted in Figure S7. The self-assembly process of the self-reporting stent may result in a slight reduction in the separation distance between the capacitor plates as the edges of the sensor may undergo some level of strain. To mitigate this effect, we aimed to maintain the capacitor plate distance at a level consistent with that of the flat 2D self-reported stent mesh.

The resonance frequency of the self-reporting stent was then measured using an external antenna connected to a vector network analyzer as the air pressure inside the tube was gradually increased from 0 to 600 mmHg by using a syringe pump. As the applied pressure increased, the displacement between the capacitor plates decreased, while the relative capacitance and resonance frequency demonstrated a strong linear relationship with the external pressure (Figure 2l,m). The linear correlation observed between the relative capacitance and resonance frequency of the self-reporting stent with external pressure substantiates the enhanced sensitivity, accuracy, and reliability. Furthermore, this relationship simplifies signal processing and data analysis. Next, the effect of external pressure on the resonance frequency of the self-reporting stent was investigated at pressure levels of 0, 50, 100, 150, 200, and 250 mmHg (Figure S8a). The results indicated that the resonance frequency decreased linearly with an increasing applied pressure. The self-reporting stent demonstrated a linear response to applied pressure, with a sensitivity of 32 kHz/mmHg (Figure S8b). The capacity of the self-reporting stent to resist radial stress is a crucial parameter in maintaining the patency of the blood vessel. Therefore, we evaluated the radial force of the self-reporting stent by using a universal tensile machine (Shumadxu, EZ-L). The radial force was applied to the self-reporting stent in the range of 0−1.4 mm at a compression rate of 0.1 mm/s (Figure 2n). The radial strength of the stent was determined by calculating the average radial force at each position. The radial force increased from 0

https://doi.org/10.1021/acssensors.3c01313
ACS Sens. 2023, 8, 4542−4553

to 0.7 N as the applied displacement increased from 0 to 1.5 mm, yielding an average radial force of 0.04 N/mm. Like other polymer-based stents, the mechanical property of our proposed self-reporting stent falls short of the desired range. The radial strength of our stent can be improved to a target range of 0.1 N/mm^2 by intercalating suitable nanofillers into the polymer matrix, enhancing its practical utility for cardiovascular applications.

The crimping process for the self-reporting stent holds significant importance, as it enables efficient stent delivery, ensures controlled expansion, and preserves structural integrity throughout the implantation procedure. The self-reporting stent was subjected to a crimping and expansion test to assess its mechanical resilience and suitability for withstanding deformation during balloon expansion, as well as its ability to promptly restore its dimensions after balloon deflation, as shown in Figure 3a,b. The self-reporting stent was mounted onto a balloon catheter and placed within a radial compression machine (Model: RJ, Blockwise) for testing. The experiments were conducted at a controlled temperature of 30 °C and a pressure of 3 bar. We measured its diameter in various states: as fabricated (control state), crimped, balloon expanded, and deflated, as shown in Figure S9. During the crimping process, the diameter of the self-reporting stent compressed from an initial 3 to 1.82 mm. Upon balloon expansion, the diameter increased to 4.1 mm, and after deflating the balloon, it recovered to 3.1 mm. These observations align with previous studies,[27,17] emphasizing that the crimping and expansion behaviors of our smart stent are comparable to those of other polymer-based stents. Our results demonstrate that the stent retains its structural integrity and shows no signs of deformation up to an expansion pressure of 3 bar.

The evaluation of the self-reporting stent for blood pressure and heart rate monitoring was conducted through a moving anthropomorphic 3D-printed phantom (Heartroid, JMC Corporation, Japan). This phantom was designed to mimic the human heart and was equipped with the proposed self-reporting stent in its coronary artery. The experimental setup further included a fractional flow reserve controller (QUANTIEN Abbot), a vector network analyzer, a wireless reader for resonance frequency measurement, and a pressure controller (Figure 3c,d). The phantom system was connected to a fractional flow reserve controller, which facilitated the detection of pressure responses from the LC-pressure sensor coupled with a wireless antenna. A commercially available thin wire-based pressure sensor (Abbot pressure wire X C12009) was utilized to measure the pressure inside the phantom (Figure 3e). This experimental setup facilitated the assessment of the self-reporting stent's efficacy under conditions that closely resemble those encountered in vivo. The impact of ambient conditions on the resonance frequency of the self-reporting stent was examined by exposing the sensor to air, deionized water, or Dulbecco's phosphate-buffered saline (DPBS) solution (Figure 3f). The frequency shift was characterized as a decrease in frequency as the environment changed from air to deionized water and then to a DPBS solution. This change in the environmental conditions resulted in not only a reduction in the resonance frequency but also a decline in the amplitude of the parameter S_{11}. The resonance frequencies of the self-reporting stent in air, deionized water, and DPBS solution were determined to be 67, 22, and 18 MHz, respectively. The observed variation in the resonance frequency is attributed to the differences in the electrochemical properties of these media, specifically the conductivity, which influences the electrical field concentration within the capacitor, leading to changes in capacitance and consequent shifts in both the resonance frequency and S_{11}. The conductivity of the DPBS solution was observed to be significantly higher (16.40 mS/cm) than that of deionized water (0.035 mS/cm), further accentuating the effects on the resonance frequency and S_{11}. To confirm the experimental data in different liquid environments such as water and DBPS, FEM simulation was carried out, and the obtained data are shown in Figure S10.

In recent years, the development of a noninvasive cuffless method to monitor blood pressure has received considerable interest since it provides a complete picture of the cardiovascular system. The developed LC-pressure sensor-integrated self-reporting stent might help people better monitor their cardiovascular health. The proposed stent can measure blood pressure continuously over the course of several hours, and the data it generates would give healthcare providers a better overall picture of blood pressure compared with the measurements with a blood pressure cuff taken a few times a day. The self-reporting stent, designed for implantation into the coronary arteries, operates in a dynamic environment of the muscle and blood. However, due to limitations, the feasibility of the self-reporting stent was evaluated using a phantom model. The influence of various environmental factors, such as air, water, and muscle, on the resonance frequency of the self-reporting stent was assessed using numerical simulation techniques (Figure S11). The dimensions of the self-reporting stent, i.e., a length and breadth of 4.2 mm and a pressure sensor width of 20 μm, were held constant. The air cavity distance was also fixed at 20 μm, and the number of inductor coils and thickness were set to 20 and 10 μm, respectively. The resonance frequency of the self-reporting stent was computed using these parameters under different environmental conditions (air, water, and muscle). The simulated resonance frequencies for air, water, and muscle were determined to be 73, 48, and 40 MHz, respectively. The results indicated that the resonance frequencies of the self-reporting stent were relatively similar in water and muscle. Accordingly, water was selected as the working environment for the phantom experiment. A pulsatile pump was used to pump water through the self-reported stent-implanted blood arteries. The pumping system mimics the systolic and diastolic pressures acting on the self-reporting stent. The beat rate was controlled by the externally applied pressure. The resonance frequency of the self-reporting stent was measured at 30, 60, and 90 beats per minute (bpm; Figure 3g). The pressures applied to maintain the beat rates of 30, 60, and 90 bpm were 42, 61, and 85 mmHg, respectively. The resonance frequency of the self-reporting stent in deionized water shifted to the lower-frequency region compared to that in the air environment. The resonance frequencies of the self-reporting stent at 30, 60, and 90 bpm were 21.81, 21.75, and 21.69 MHz, respectively. The sensitivity of the self-reported stent was about 3.5 kHz/mmHg. The real-time traces of the resonance frequency for applied beat rates are provided in Videos S1, S2, S3, S4. To demonstrate its practical feasibility, the proposed self-reporting stent was attached radially to the blood vessels on top of the wrist (Figure S12). Video S5 shows the real-time response of the radial pulse rate on the wrist.

The resonance frequencies measured using a vector network analyzer, according to systole and diastole, were found to be

https://doi.org/10.1021/acssensors.3c01313
ACS Sens. 2023, 8, 4542−4553

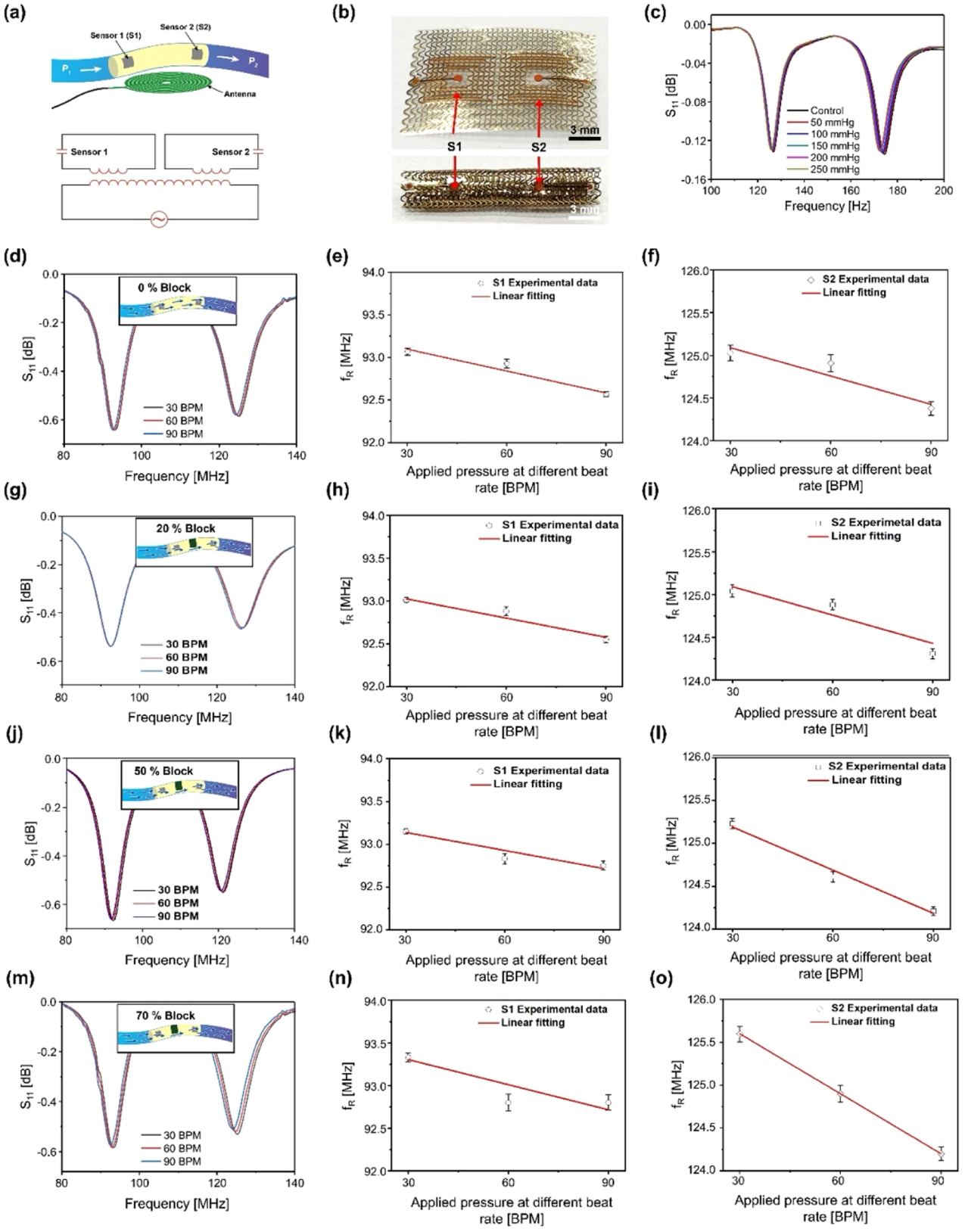

Figure 4. Blood flow monitoring and the detection of occlusion formation using a dual-pressure-sensor-infused self-reporting stent. (a) Illustration of the artificial blood arteries implanted with a dual-sensor-infused self-reporting stent connected to an external wireless reader. (b) Optical images of the dual-pressure-sensor-infused self-reporting stent before and after the self-assembly process. (c) Resonance frequency of the dual-sensor-infused self-reporting stent at different applied pressures. (d, g, j, m) Resonance frequency of the dual-pressure-sensor-infused self-reporting stent before and after different occlusions of 70, 50, and 20% with indicated pulse rates. (e−o) Linear plots illustrating the relationship between the applied pressure and the changes in the resonance frequency of the dual-sensor-integrated self-reporting stent in sensor 1 and sensor 2 regions before and after the formation of occlusion.

https://doi.org/10.1021/acssensors.3c01313
ACS Sens. 2023, 8, 4542−4553

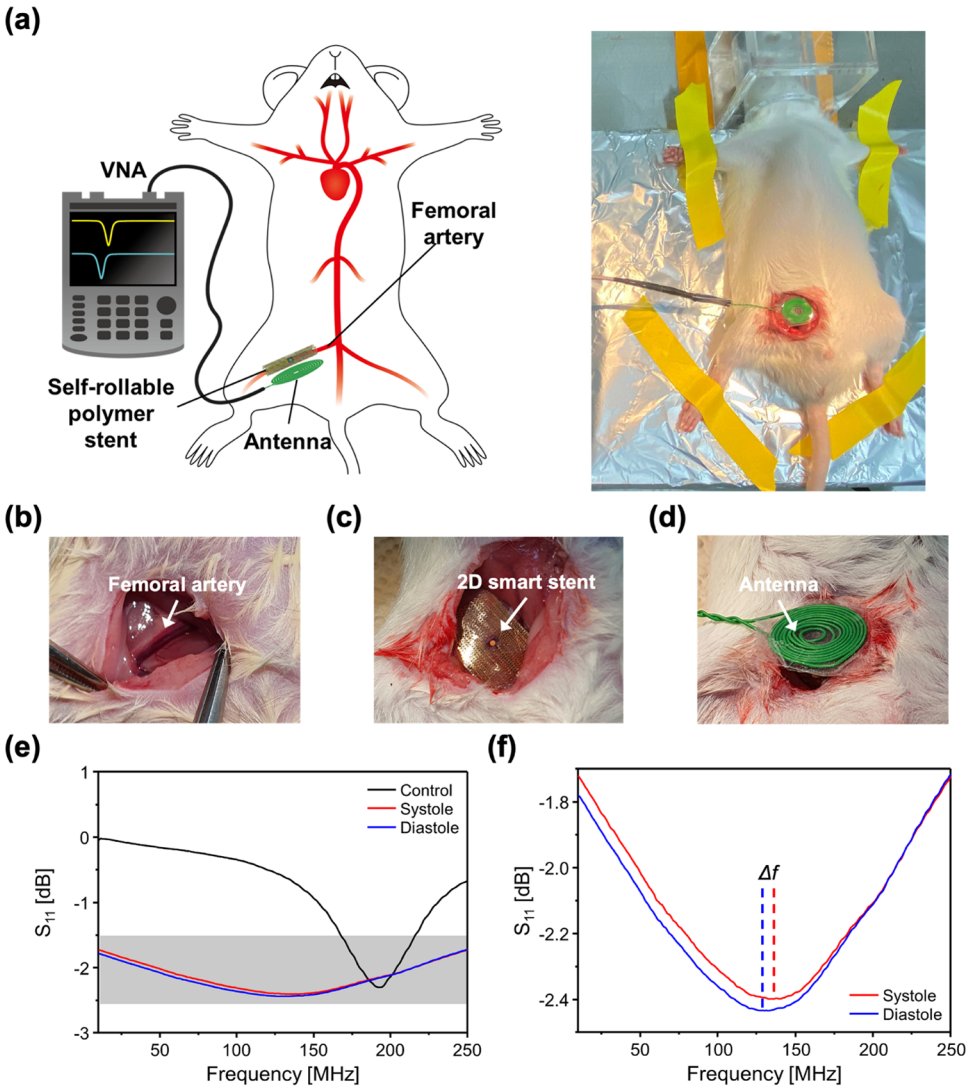

Figure 5. In vivo analysis of the proposed self-reporting stent. (a) Schematic showing the experimental protocol of the self-reporting stent implanted in a 5 week old Sprague-Dawley rat. The resonance frequency of the self-reporting stent according to the systole and diastole was measured by using a vector network analyzer coupled with an external wireless reader. (b−d) Photographs taken at various stages of the implantation process of the self-reporting stent into the femoral artery of a 5 week old Sprague−Dawley rat. (e) Resonance frequency of the implanted self-reporting stent during diastole and systole of pressure acting on the femoral artery of the Sprague-Dawley rat. (f) Magnified view of the resonance frequency shift of the self-reporting stent at diastole and systole of the femoral artery.

34.56 and 34.61 MHz, respectively. The proposed self-reporting stent was used for continuous monitoring of beating frequency and pressure using a phantom system, as demonstrated in Figure 3h−j. The beating frequency was controlled by the externally applied pressure using a pumping system that mimics the systolic and diastolic pressures acting on the self-reporting stent. By detecting changes in the resonance frequency of the stent during continuous measurement at 30 bpm, the proposed device is able to produce stable and reliable results, indicating its high precision in detecting cardiac activities. This demonstrates the potential of the self-reporting stent to provide accurate and continuous monitoring of important cardiovascular parameters in vivo. The sensitivity of the proposed self-reporting stent in air and blood was 2 and 1 cm, respectively. This is significantly higher than the sensitivities of previously reported polymer-based smart stents, showcasing the exceptional sensitivity of our proposed device, as shown in Table S1.

Self-reporting stents have been developed to measure blood pressure and resting blood pressure at specific locations within the cardiovascular system. However, the current technology is limited in its ability to provide a complete picture of blood flow due to the presence of only one pressure sensor at the center of the stent. Measuring blood flow at the restenosis site is essential to obtaining a more comprehensive understanding of cardiovascular health. To address this limitation, a new design of a self-reporting stent with two integrated pressure sensors has been proposed. The use of two sensors is made possible by the larger size of the inductor coil in this new design. The integration of two sensors in a self-reporting stent improves its measurement capabilities by providing a more accurate assessment of in-stent restenosis with blood pressure and blood flow data. Therefore, we incorporated two sensors into the stent structure and tested their response to a range of pressures in a moving anthropomorphic 3D-printed phantom (Figure 4a). The optical images of the self-reporting stent before and after self-assembly are shown in Figure 4b. The

https://doi.org/10.1021/acssensors.3c01313
ACS Sens. 2023, 8, 4542−4553

change in the resonance frequency of the dual sensors was measured at various pressure levels (Figure 4c). The mesh structure of the dual-sensor-infused self-reporting stent exhibited a resonance frequency of 126 MHz for sensor 1 and 176 MHz for sensor 2. The ability of the reader to detect the resonance frequency at a distance of 16 mm can be observed in both of the dual sensors within the stent structure, as shown in Figure S13a. The sensitivity of the dual-sensor-infused self-reporting stent was investigated according to the external antenna reading distance. The intensities of the resonance frequency of both sensors infused in the self-reporting stent decreased with an increasing external reading distance owing to the decrease in the coupling effect. Despite the observed decrease in the resonance frequency with an increasing working antenna distance, the sensitivity of the dual-sensor-infused self-reporting stent was found to be remarkable. The resonance frequency of the stent was found to decrease gradually with increasing pressure (Figure S13b,c). Both sensors in the self-reporting stent were responsive to the applied pressure, leading to changes in the resonance frequency.

The detection of occlusions in the coronary arteries using stents is crucial for improving patient outcomes and reducing the risk of cardiac events, as they can lead to several adverse cardiac events such as myocardial infarction and angina. Early and accurate detection of an occlusion allows prompt intervention, which can improve patient outcomes and reduce the risk of long-term cardiac damage. The use of stents for detecting occlusion in coronary arteries enables minimally invasive and real-time monitoring of a patient's condition. Therefore, we evaluated the performance of the dual-sensor self-reporting stent in the detection of different occlusions of 20, 50, and 70% in the coronary artery of a moving anthropomorphic 3D-printed phantom (inset: Figures 4d,g,j,m and S14). The occlusions were artificially induced in the coronary artery of the moving 3D-printed phantom, and the resonance frequency of the dual-sensor-infused self-reporting stent was measured in the absence and presence of different occlusions at applied pressures of 30, 60, and 90 bpm (Figure 4d,g,j,m). The resonance frequencies of the first sensor changed from 93.07, 92.93, and 92.57 MHz (before occlusion) to 93.33, 92.81, and 92.61 MHz (after 70% occlusion) at applied pressures of 30, 60, and 90 bpm, respectively (Figure 4e,h). The resonance frequencies of the second sensor were measured as 125.03, 124.91, and 124.38 MHz before occlusion and 125.61, 124.91, and 124.21 MHz after a 70% occlusion at 30, 60, and 90 bpm, respectively (Figure 4f,i). Following this, when the occlusion reached 50%, the resonance frequency of the first sensor changed to 93.15, 92.83, and 92.75 MHz (Figure 4k), while the second sensor's resonance frequency changed to 125.23, 124.5, and 124.68 MHz (Figure 4l), respectively. No changes in the resonance frequency were observed after a 20% occlusion for both the first and second sensors (Figure 4n,o). This data demonstrates that the dual sensors integrated into the stent can detect blockages of up to 50%, while blockages of 20% or less remain undetected. Overall, these observations suggest that the proposed dual-sensor-infused self-reporting stent enhances the accuracy and reliability of the occlusion detection system by incorporating sensors that can provide real-time data about the patient's cardiac condition. The calculated flow rates for 30, 60, and 90 bpm were 1.308, 1.548, and 1.826 L/min, respectively.

The biocompatibility and practicality of the proposed self-reporting stent were evaluated in vivo through an animal experiment performed on a 5 week old Sprague−Dawley (SD) rat. In this particular in vivo experiment, due to the small diameter of the rat's femoral artery, it did not match the crimped diameter of the fabricated self-reporting stent. Achieving a full wraparound coverage of the femoral artery with the fabricated self-reporting stent was challenging, as there were frequent gaps between the sensor and the artery. To detect minor pressure changes effectively, we opted to conduct an in vivo experiment using the smart stent in its flat state. To maintain a consistent and secure contact between the sensor and the femoral artery, a tissue adhesive biological glue (Histoacryl, Braun, Germany) was used. The resonance frequency of the self-reporting stent was measured using an external antenna connected to a portable network analyzer (N9913B, Keysight), and the change in the resonance frequency was monitored to investigate the blood pressure (Figure 5a,b). C-reactive protein (CRP) is a protein secreted by the liver in response to inflammation. A highly sensitive CRP (hs-CRP) test and a standard CRP test were performed to assess the potential allergic reactions in the SD rat 1 month after the implantation of the self-reporting stent. Serum CRP levels were less than 0.15 mg/L, indicating a low-risk level, while standard CRT levels were less than 0.1 mg/dL (Table S2). The resonance frequencies of the implanted self-reporting stent during diastole and systole were found to be 136 and 129 MHz, respectively (Figure 5c,d). The S_{11} amplitude of the self-reporting stent measured in the in vivo experiment with the SD rat was lower than the resonance frequency measured in the phantom experiment. In vivo animal experiment demonstrates the real-time changes in the resonance frequency of the sensor according to the femoral artery pulse rate of SD rats, as shown in Video S6. The observed beat rate was slightly lower than the real heart rate of the rat model (>4 bpm). This difference may be attributed to the induction of anesthesia with propofol, which is often associated with a significant decrease in arterial blood pressure and heart rate. This could be attributed to the 10 mm distance between the external loop antenna and the self-reporting stent, which significantly decreased S_{11}.

In summary, the proposed self-reporting stent was fabricated by using modified photolithography techniques with SU-8 and Cu. Both materials are commercially available and have been employed in various biomedical devices due to their biocompatibility and mechanical stability. The photolithography-based process used in this study is inherently scalable. Large-scale production can be achieved by adopting techniques such as wafer-level processing where hundreds of devices can be fabricated on a single wafer. This mass production capability can significantly reduce the cost per device, making it economically viable. Furthermore, the design of our stent is adaptable. By tweaking the photomask design, stents of different sizes and specifications can be manufactured without significant changes in the fabrication process. This adaptability ensures that the stent can provide a broader range of vascular diameters and conditions. Before clinically translating the proposed self-reporting stent, it is crucial to conduct extensive in vivo tests to confirm the device's safety and efficacy. While our current study establishes the foundation, rigorous preclinical and clinical trials will be the next steps. Collaboration with medical professionals will provide insights into real-world challenges and ensure that our device aligns with clinical standards.

https://doi.org/10.1021/acssensors.3c01313
ACS Sens. 2023, 8, 4542−4553

CONCLUSIONS

We have realized the dual-sensor-infused self-reporting stent for the detection of stent restenosis, blood pressure, and blood flow inside the coronary arteries. The inductance and resonance frequency of the self-reported stent were simulated by using the finite element method to achieve the desired self-reported stent design. The self-reporting stent was fabricated by using a modified photolithography technique, thermal bonding, and temperature-induced self-assembly process. The entire surface of the stent strut was utilized for the inductor coil. The encapsulation of a larger inductor coil on the entire stent strut area enabled the integration of two pressure sensors in the same stent and provided excellent sensitivity, efficiently transferring biological cues to the external wireless reader. The proposed self-reporting stent with two sensors demonstrated a 2-fold improvement in sensing resolution compared to a previously reported self-reporting stent due to the utilization of a large-area inductor coil. The feasibility of the proposed self-reporting stent was demonstrated through the measurement of blood pressure and heart rate by implanting the stent into the blood vessels of a 3D-printed phantom simulating the human heart. The results of the in vivo analysis verified the biocompatibility and multiple functionalities of the proposed self-reporting stent. The integration of a dual-sensor system into a single stent structure improved the accuracy and reliability of the collected data. Based on the obtained results, we sincerely believe that the proposed technology has the potential to improve patient outcomes by allowing the early detection and treatment of blood pressure changes, reducing the risk of complications, and improving the quality of life for patients.

ASSOCIATED CONTENT

Supporting Information

The Supporting Information is available free of charge at https://pubs.acs.org/doi/10.1021/acssensors.3c01313.

Detailed fabrication process flow; characterization technique; effect of inductor turns in LC-pressure sensor; information about sensor's working conditions; and a table presenting post-in vivo experimental data (PDF)

Real-time traces of the resonance frequency for applied beat rates (Video S1) (MOV)

Real-time traces of the resonance frequency for applied beat rates (30 bpm) (Video S2) (MOV)

Real-time traces of the resonance frequency for applied beat rates (60 bpm) (Video S3) (MOV)

Real-time traces of the resonance frequency for applied beat rates (90 bpm) (Video S4) (MOV)

Real-time response of the radial pulse rate on the wrist (Video S5) (MOV)

In vivo animal experiment demonstrates the real-time changes in the resonance frequency of the sensor according to the femoral artery pulse rate of SD rats (Video S6) (MP4)

AUTHOR INFORMATION

Corresponding Author

Dong-Weon Lee − *School of Mechanical Engineering, Chonnam National University, Gwangju 61186, Republic of Korea; Green Energy & Nano Technology R&D Group, Korea Institute of Industrial Technology (KITECH), Gwangju 61012, Republic of Korea; Center for Next-Generation Sensor Research and Development, Chonnam National University, Gwangju 61186, Republic of Korea;* orcid.org/0000-0002-6624-6949; Email: mems@jnu.ac.kr

Authors

Nomin-Erdene Oyunbaatar − *School of Mechanical Engineering, Chonnam National University, Gwangju 61186, Republic of Korea; Advanced Medical Device Research Center for Cardiovascular Disease, Chonnam National University, Gwangju 61186, Republic of Korea*

Dong-Su Kim − *School of Mechanical Engineering, Chonnam National University, Gwangju 61186, Republic of Korea; Green Energy & Nano Technology R&D Group, Korea Institute of Industrial Technology (KITECH), Gwangju 61012, Republic of Korea*

Arunkumar Shanmugasundaram − *School of Mechanical Engineering, Chonnam National University, Gwangju 61186, Republic of Korea; Advanced Medical Device Research Center for Cardiovascular Disease, Chonnam National University, Gwangju 61186, Republic of Korea*

Su-Hwan Kim − *School of Electrical Engineering, Korea Advanced Institute of Science and Technology, Daejeon 34141, Republic of Korea*

Yun-Jin Jeong − *School of Mechanical Engineering, Chonnam National University, Gwangju 61186, Republic of Korea; Advanced Medical Device Research Center for Cardiovascular Disease, Chonnam National University, Gwangju 61186, Republic of Korea*

Juyeong Jo − *Korea Institute of Medical Microrobotics, Gwangju 61011, Republic of Korea*

Kyeongha Kwon − *School of Electrical Engineering, Korea Advanced Institute of Science and Technology, Daejeon 34141, Republic of Korea*

Eunpyo Choi − *School of Mechanical Engineering, Chonnam National University, Gwangju 61186, Republic of Korea; Korea Institute of Medical Microrobotics, Gwangju 61011, Republic of Korea*

Complete contact information is available at: https://pubs.acs.org/10.1021/acssensors.3c01313

Notes

The authors declare no competing financial interest.

ACKNOWLEDGMENTS

This study was supported by a National Research Foundation of Korea (NRF) grant funded by the Korean government (MSIT) (2020R1A5A8018367) through the National Research Foundation of Korea (NRF).

REFERENCES

(1) World Health Organization. Cardiovascular Disease. 2017. http://www.who.int/cardiovascular_diseases/en/.

(2) Santulli, G. Epidemiology of Cardiovascular Disease in the 21st Century: Updated Numbers and Updated Facts *J. Cardiovasc. Dis. Res.* 2013; Vol. *1*.

(3) Rauch, U.; Osende, J. I.; Fuster, V.; Badimon, J. J.; Fayad, Z.; Chesebro, J. H. Thrombus Formation on Atherosclerotic Plaques: Pathogenesis and Clinical Consequences. *Ann. Intern. Med.* **2001**, *134*, 224−238.

(4) Anderson, T. J.; Grégoire, J.; Pearson, G. J.; Barry, A. R.; Couture, P.; Francis, G. A.; Genest, J.; Grover, S. A.; Gupta, M.; et al. Canadian Cardiovascular Society Guidelines for the Management of

Dyslipidemia for the Prevention of Cardiovascular Disease in the Adult. *Can. J. Cardiol.* **2016**, *32*, 1263−1282, DOI: 10.1016/j.cjca.2016.07.510.
(5) Bønaa, K. H.; Mannsverk, J.; Wiseth, R.; Aaberge, L.; Myreng, Y.; Nygård, O.; Nilsen, D. W.; Kløw, N. E.; Uchto, M.; Trovik, T.; Bendz, B. Drug-Eluting or Bare-Metal Stents for Coronary Artery Disease. *N. Engl. J. Med.* **2016**, *375*, 1242−1252, DOI: 10.1056/NEJMoa1607991.
(6) Borhani, S.; Hassanajili, S.; Ahmadi Tafti, S. H.; Rabbani, S. Cardiovascular Stents: Overview, Evolution, and Next Generation. *Prog. Biomater.* **2018**, *7*, 175−205.
(7) Moeri, L.; Lichtenberg, M.; Gnanapiragasam, S.; Barco, S.; Sebastian, T. Braided or Laser-Cut Self-Expanding Nitinol Stents for the Common Femoral Vein In Patients With Post-Thrombotic Syndrome. *J. Vasc. Surg.: Venous Lymphat. Disord.* **2021**, *9*, 760−769.
(8) Coughlan, J. J.; Maeng, M.; Räber, L.; Brugaletta, S.; Aytekin, A.; Jensen, L. O.; Bär, S.; Ortega-Paz, L.; Laugwitz, K. L.; Madsen, M.; Heg, D.; et al. Ten-Year Patterns of Stent Thrombosis after Percutaneous Coronary Intervention with New-Versus Early-Generation Drug-Eluting Stents: Insights from the DECADE cooperation. *Rev. Esp. Cardiol. (Engl. Ed.)* **2022**, *75*, 894−902, DOI: 10.1016/j.rec.2022.02.003.
(9) Zhong, P. Y.; Shang, Y. S.; Bai, N.; Ma, Y.; Niu, Y.; Wang, Z. L. Dual Antiplatelet Therapy After Drug-Eluting Stents Implantation in East Asians: a Network Meta-Analysis of Randomized Controlled Trials. *J. Cardiovasc. Pharmacol.* **2022**, *80*, 216−225.
(10) Oliver, A. A.; Sikora-Jasinska, M.; Demir, A. G.; Guillory, R. J., II Recent Advances and Directions in the Development of Bioresorbable Metallic Cardiovascular Stents: Insights from Recent Human and In Vivo Studies. *Acta Biomater.* **2021**, *127*, 1−23, DOI: 10.1016/j.actbio.2021.03.058.
(11) Di Mario, C.; Griffiths, H. U. W.; Goktekin, O.; Peeters, N.; Verbist, J. A. N.; Bosiers, M.; Deloose, K.; Heublein, B.; Rohde, R.; Kasese, V.; Ilsley, C.; Erbel, R. Drug-Eluting Bioabsorbable Magnesium Stent. *J. Interventional Cardiol.* **2004**, *17*, 391−395, DOI: 10.1111/j.1540-8183.2004.04081.x.
(12) Mehran, R.; Dangas, G.; Abizaid, A. S.; Mintz, G. S.; Lansky, A. J.; Satler, L. F.; Pichard, A. D.; Kent, K. M.; Stone, G. W.; Leon, M. B. Angiographic Patterns of In-Stent Restenosis: Classification and Implications for Long-Term Outcome. *Circulation* **1999**, *100*, 1872−1878.
(13) Stanziale, S. F.; Wholey, M. H.; Boules, T. N.; Selzer, F.; Makaroun, M. S. Determining In-Stent Stenosis of Carotid Arteries by Duplex Ultrasound Criteria. *J. Endovasc. Ther.* **2005**, *12*, 346−353.
(14) Gulari, M. N.; Ghannad-Rezaie, M.; Novelli, P.; Chronis, N.; Marentis, T. C. An Implantable X-Ray-Based Blood Pressure Microsensor for Coronary In-Stent Restenosis Surveillance and Prevention. *J. Microelectromech. Syst.* **2015**, *24*, 50−61.
(15) Luo, Y.; Chen, X.; Dahmardeh, M.; Takahata, K. RF-Powered Stent with Integrated Circuit Breaker for Safeguarded Wireless Hyperthermia Treatment. *J. Microelectromech. Syst.* **2015**, *24*, 1293−1302.
(16) Hoare, D.; Bussooa, A.; Neale, S.; Mirzai, N.; Mercer, J. The Future of Cardiovascular Stents: Bioresorbable and Integrated Biosensor Technology. *Adv. Sci.* **2019**, *6*, No. 1900856.
(17) Herbert, R.; Mishra, S.; Lim, H. R.; Yoo, H.; Yeo, W. H. Fully Printed, Wireless, Stretchable Implantable Biosystem toward Batteryless, Real-Time Monitoring of Cerebral Aneurysm Hemodynamics. *Adv. Sci.* **2019**, *6*, No. 1901034.
(18) Son, D.; Lee, J.; Lee, D. J.; Ghaffari, R.; Yun, S.; Kim, S. J.; Lee, J. E.; Cho, H. R.; Yoon, S.; Yang, S.; Lee, S.; et al. Bioresorbable Electronic Stent Integrated with Therapeutic Nanoparticles for Endovascular Diseases. *ACS Nano* **2015**, *9*, 5937−5946.
(19) Chen, J.; Yi, Y.; Selvaraj, M.; Takahata, K. Experimental Analysis on Wireless Heating of Resonant Stent for Hyperthermia Treatment of In-Stent Restenosis. *Sens. Actuators, A* **2019**, *297*, No. 111527.
(20) Oyunbaatar, N. E.; Kim, D. S.; Prasad, G.; Jeong, Y. J.; Lee, D. W. Self-Rollable Polymer Stent Integrated with Wireless Pressure Sensor for Real-time Monitoring of Cardiovascular Pressure. *Sens. Actuators, A* **2022**, *346*, No. 113869.
(21) Chen, X.; Brox, D.; Assadsangabi, B.; Ali, M. S. M.; Takahata, K. A Stainless-Steel-based Implantable Pressure Sensor Chip and its Integration By Microwelding. *Sens. Actuators, A* **2017**, *257*, 134−144.
(22) Park, J.; Kim, J. K.; Patil, S. J.; Park, J. K.; Park, S.; Lee, D. W. A Wireless Pressure Sensor Integrated with a Biodegradable Polymer Stent for Biomedical Applications. *Sensors* **2016**, *16*, No. 809, DOI: 10.3390/s16060809.
(23) Yi, Y.; Wang, B.; Li, C. Sensors-based Monitoring and Treatment Approaches for In-Stent Restenosis. *J. Biomed. Mater. Res., Part B* **2023**, *111*, 490−498.
(24) Takahata, K.; Gianchandani, Y. B.; Wise, K. D. Micromachined Antenna Stents and Cuffs for Monitoring Intraluminal Pressure and Flow. *J. Microelectromech. Syst.* **2006**, *15*, 1289−1298.
(25) Park, J.; Kim, J. K.; Kim, D. S.; Shanmugasundaram, A.; Park, S. A. S.; Kang, S. A.; Kim, S. H.; Jeong, M. H.; Lee, D. W. Wireless Pressure Sensor Integrated with a 3D Printed Polymer Stent for Smart Health Monitoring. *Sens. Actuators, B* **2019**, *280*, 201−209.
(26) Green, S. R.; Kwon, R. S.; Elta, G. H.; Gianchandani, Y. B. In Situ and Ex Vivo Evaluation of a Wireless Magnetoelastic Biliary Stent Monitoring System. *Biomed. Microdevices* **2010**, *12*, 477−484.
(27) Herbert, R.; Elsisy, M.; Rigo, B.; Lim, H. R.; Kim, H.; Choi, C.; Kim, S.; Ye, S. H.; Wagner, W. R.; Chun, Y.; Yeo, W. H. Fully Implantable Batteryless Soft Platforms with Printed Nanomaterial-based Arterial Stiffness Sensors for Wireless Continuous Monitoring of Restenosis in Real Time. *Nano Today* **2022**, *46*, No. 101557.
(28) Chen, X.; Brox, D.; Assadsangabi, B.; Hsiang, Y.; Takahata, K. Intelligent telemetric stent for wireless monitoring of intravascular pressure and it's in vivo testing. *Biomed. Microdevices* **2014**, *16*, 745−759.
(29) Chen, X.; Assadsangabi, B.; Hsiang, Y.; Takahata, K. Enabling Angioplasty-Ready "Smart" Stents to Detect In-Stent Restenosis and Occlusion. *Adv. Sci.* **2018**, *5*, No. 1700560, DOI: 10.1002/advs.201700560.
(30) Kim, D. S.; Oyunbaatar, N. E.; Shanmugasundaram, A.; Jeong, Y. J.; Park, J.; Lee, D. W. Stress Induced Self-Rollable Smart-Stent-based U-Health Platform for In-Stent Restenosis Monitoring. *Analyst* **2022**, *147*, 4793−4803.
(31) Chen, P. J.; Saati, S.; Varma, R.; Humayun, M. S.; Tai, Y. C. Wireless Intraocular Pressure Sensing Using Microfabricated Minimally Invasive Flexible-Coiled LC Sensor Implant. *J. Microelectromech. Syst.* **2010**, *19*, 721−734.
(32) Lee, H.; Cook, B. S.; Murali, K. P.; Raj, M.; Tentzeris, M. M. Inkjet Printed High-Q RF Inductors on Paper Substrate with Ferromagnetic Nanomaterial. *IEEE Microwave Wireless Compon. Lett.* **2016**, *26*, 419−421.
(33) Ahn, D.; Hong, S. Effect of Coupling Between Multiple Transmitters or Multiple Receivers on Wireless Power Transfer. *IEEE Trans. Ind. Electron.* **2013**, *60*, 2602−2613.